Using NWP Simulations in Satellite Rainfall Estimation of Heavy Precipitation Events over Mountainous Areas

XINXUAN ZHANG, EMMANOUIL N. ANAGNOSTOU, AND MARIA FREDIANI

Department of Civil and Environmental Engineering, University of Connecticut, Storrs, Connecticut

STAVROS SOLOMOS AND GEORGE KALLOS

School of Physics, University of Athens, Athens, Greece

(Manuscript received 29 November 2012, in final form 9 June 2013)

ABSTRACT

In this study, the authors investigate the use of high-resolution simulations from the Weather Research and Forecasting Model (WRF) for evaluating satellite rainfall biases of flood-inducing storms in mountainous areas. A probability matching approach is applied to evaluate a power-law relationship between satellite-retrieved and WRF-simulated rain rates over the storm domain. Satellite rainfall in this study is from the NOAA Climate Prediction Center morphing technique (CMORPH). Results are presented based on analyses of five heavy precipitation events that induced flash floods in northern Italy and southern France complex terrain basins. The WRF-based adjusted CMORPH rain rates exhibited improved error statistics against independent radar rainfall estimates. The authors show that the adjustment procedure reduces the underestimation of high rain rates, thus moderating the magnitude dependence of CMORPH rainfall bias. The Heidke skill score for the WRF-based adjusted CMORPH was consistently higher for a range of rain rate thresholds. This is an indication that the adjustment procedure ameliorates the satellite rain rates to provide a better estimation. Results also indicate that the low rain detection of CMORPH technique is also identifiable in the WRF–CMORPH comparison; however, the adjustment procedure herein does not incorporate this effect on the satellite rainfall bias adjustment.

1. Introduction

Heavy precipitation events (HPE) occurring over mountainous regions have a tendency to trigger devastating flash floods with consequential hazards such as landslides or debris flows (e.g., Malguzzi et al. 2006; Petrucci and Polemio 2009). These effects substantially impact society, which is in need of better forecasting tools to support early warning (e.g., Ruin et al. 2008; Schelfaut et al. 2011). Flash flood forecasting has been a very important topic in hydrologic research. One of the crucial prerequisites for establishing a reliable hydrologic modeling for flash floods is to gather accurate precipitation data for the flood simulation. However, there is no precipitation measurement method that would provide accurate rainfall estimates over extensive areas. Generally, the network of rain gauges furnishes the most accurate observation, but at discrete locations it cannot represent the rainfall processes over large domains, particularly when this includes complex topography. Radar-derived precipitation is considered the most reliable data source for obtaining area rainfall estimates when it is based on a combination of error correction procedures, including adjustments for mean field bias using rain gauges. However, the area covered by radar networks is still limited, particularly over complex terrain where the radar measurements may encounter beam blockage and vertical reflectivity profile effects (Maddox et al. 2002). Satellite-retrieved precipitation data can cover large regions globally, but they are affected by significant uncertainty since the satellite observation is often influenced by the atmospheric or land surface effects and other technical factors (Tang and Hossain 2012).

There is a broad consensus being demonstrated by many researches that high-intensity rainfall rates tend to be underestimated by satellite retrievals, especially over

Corresponding author address: Emmanouil Anagnostou, Civil and Environmental Engineering, University of Connecticut, Storrs, CT 06269.
E-mail: manos@engr.uconn.edu

DOI: 10.1175/JHM-D-12-0174.1

complex topography (Prat and Barros 2010; Kidd et al. 2012; Bitew et al. 2012). Comparing different satellite products in the upper Blue Nile area of Ethiopia, Bitew et al. (2012) have indicated that microwave-based satellite rainfall retrievals may have better accuracies over mountainous areas than infrared-based satellite rainfall estimates. Similarly, Dinku et al. (2007) have shown that the National Oceanic and Atmospheric Administration (NOAA) Climate Prediction Center (CPC) morphing technique (CMORPH) exhibits the best consistency among 10 different satellite rainfall products with area-averaged gauge rainfall over complex topography.

Although the satellite rainfall is associated with significant uncertainty, it is worth investigating the feasibility of using these estimates as input to hydrologic models, given that satellites have the spatial coverage advantage over rain gauges and radar observations, particularly over mountainous areas. Bitew et al. (2012) examined several satellite rainfall products as input to a hydrological model and found that all streamflow simulations had strong underestimation. Similarly, Nikolopoulos and Anagnostou (2010) tested the performance of satellite rainfall products at different resolutions for flood modeling on a range of basin scales using a distributed hydrologic model. In all flood simulations, the 8 km/hourly resolution CMORPH rainfall product provided better error metrics than the coarser (25 km, 3 hourly) satellite rainfall products.

In a recent study, Nikolopoulos et al. (2012) applied bias adjustment on three of the current high-resolution (4 km, hourly; 8 km, hourly; and 25 km, 3 hourly) satellite rainfall products using rain gauge–adjusted (1 km, hourly) radar rainfall data over northeast Italy. They subsequently forced a distributed hydrologic model with both the original and adjusted satellite products and the reference radar rainfall to simulate a major flash flood over a 600-km^2 basin. They showed that neither satellite product could lead the hydrologic simulations to capture the magnitude of the flood event, which indicated that the adjustment procedures need to be meliorated or the satellite rainfall adjustments need to be improved, according to the local topography conditions.

Besides the precipitation observation methods, quantitative rainfall forecasts from numerical weather prediction (NWP) models can be employed by a hydrological model for generating flood predictions. Nevertheless, the accuracy of precipitation fields derived from NWP forecasts suffers from spatiotemporal and amplitude errors depending on the model physics, dynamics, and model configuration (Schwartz et al. 2010; Bray et al. 2011). Generally, NWP initialized with analysis data can provide a reliable estimation of the synoptically forced rainfall, while satellite observations can better represent the convective rainfall temporal variability (Ebert et al. 2007).

Since each precipitation data source has its own advantages and shortcomings, it is possible to combine the different types of precipitation estimates for the purpose of acquiring data with higher accuracy. For example, Papadopoulos et al. (2008) reported better simulation results from an NWP model using radar rainfall data to substitute the rainfall forcing of the model's land surface scheme. Huffman et al. (1995) have used numerical model predictions to fill data voids in their merged satellite products. Recently, Zupanski et al. (2011) used the Weather Research and Forecasting Model (WRF) with data assimilation to downscale satellite rainfall estimates for hydrological applications. Their results were demonstrated for Tropical Storm Erin, showing that the WRF Ensemble Data Assimilation System can lead to improved high-resolution precipitation estimates when adding satellite observations into the system.

This study proposes a new approach to blending NWP with satellite rainfall estimation, namely, using the rainfall magnitude derived from high-resolution NWP simulations to evaluate the overall satellite rainfall bias over complex topography. The focus is on heavy precipitation storms that cause flash floods in small- to medium-sized basins. The study uses high-quality, gauge-adjusted radar rainfall estimates from five heavy precipitation storm cases to evaluate the performance of the proposed approach applied on the CMORPH (8 km/half hourly) satellite rainfall product, selected because of its better consistency, among other satellite products, over complex topography. High-resolution NWP storm simulations are performed using WRF (Skamarock et al. 2008). A description of the study area and data sources are provided in section 2, followed by description of the WRF setup in section 3. Section 4 describes the methodology of the adjustment procedure. Section 5 discusses the results for the different storm cases, and conclusions are provided in section 6.

2. Study area and data

a. Study area

Three areas (Fig. 1) associated with complex topography are selected for this study. These regions are located in the Italian Alps and the Massif Central mountain range that exhibit frequent heavy precipitation and floods. A recent study (Mehta and Yang 2008) about the Mediterranean basin indicates that heavy precipitation has peak frequency and accumulation over the mountainous regions according to satellite measurements. The areas along the Alpine foothills and the southern flanks of the

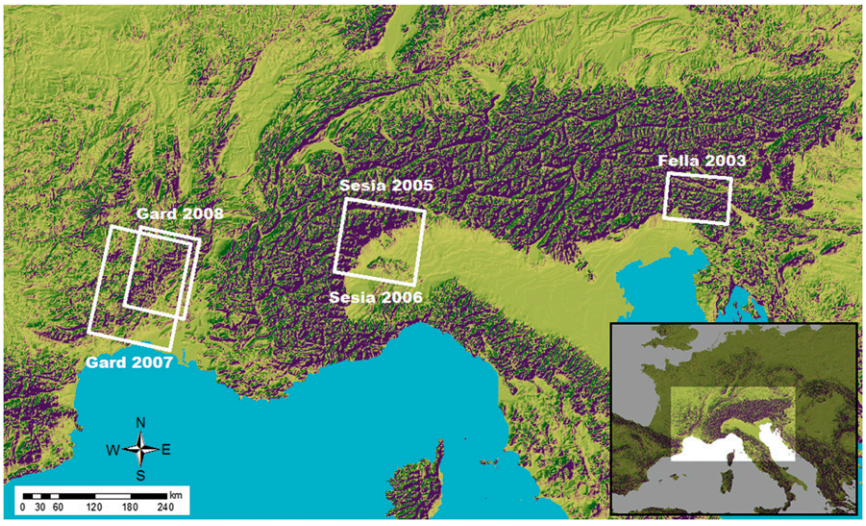

FIG. 1. Study areas: (left) Gard radar domains for Gard2007 and Gard2008 cases, (middle) Sesia radar domain for Sesia2005 and Sesia2006 cases, and (right) Fella radar domain for Fella2003 case.

Massif Central mountains are particularly under the influence of extreme rain accumulations because the air from the Mediterranean Sea brings sufficient moisture and the mountain windward slope helps the lifting condensation process, therefore leading to heavy rains and snow storms (Frei and Schar 1998; Nuissier et al. 2008).

Five heavy precipitation events in northern Italy and southern France that produced flash floods in three medium-sized basins (shown in Fig. 1)—Fella and Sesia in northern Italy and Gard in southern France—are selected to evaluate quantitative precipitation estimation by CMORPH satellite retrieval and potential improvements gained by adjusting those estimates using high-resolution rainfall simulations from WRF. Evaluation of the rainfall estimates is based on high-quality, rain gauge–calibrated radar rainfall fields, which is discussed in the next section.

The Fella area is located at the Friuli–Venezia Giulia region in northeastern Italy adjacent to northwestern Slovenia and southern Austria. The area represents sub-Mediterranean alpine climate. This type of climate exhibits more humid summer than the typical Mediterranean climate. The Sesia area is located in northwestern Italy. It contains the Sesia River basin and is featured by unique topographies. The bottom-right part of the study area is the Alpine foreland region, while the top-left part includes a portion of the central chain of western Alps. This region also belongs to the sub-Mediterranean zone and exhibits a similar climate type as the Fella. The Gard area, on the other hand, is located in south-central France, over the southeastern edge of the Massif Central mountain range. Although the elevation of this area is the highest among the Massif Central mountain range, it is still much lower than the main Alps chain. This represents a typical Mediterranean climate featured by hot, dry summers and cool, wet winters (Lionello et al. 2006). The fall season in the area exhibits the highest rainfall rates and accumulations

TABLE 1. Storm events information.

Events	Fella2003	Sesia2005	Sesia2006	Gard2007	Gard2008
Location	Fella	Sesia	Sesia	Gard	Gard
Starting time	29 Aug 2003 0900 UTC	1 Aug 2005 1800 UTC	14 Sep 2006 0000 UTC	19 Nov 2007 0600 UTC	31 Oct 2008 0600 UTC
Duration (h)	12	24	47	96	48
Radar maximum total rainfall (mm)	343	253	353	294	409
Radar mean rain rates (mm h^{-1})	8.8	2.6	4.1	2.1	3.7
Percentage of grids having heavy precipitation ($\geq$10 mm h^{-1})	20%	2.8%	4.3%	0.9%	5.3%

TABLE 2. Data resolution.

Dataset	Special resolution	Temporal resolution
CMORPH	8 km	0.5 h
Radar	1 km	1 h
WRF	2 km	1 h

because of frontal systems and mesoscale convective systems (MCSs) occurring in the area.

b. Precipitation data

Table 1 summarizes the basic information of the five storm events used in this study. The durations of these events vary from 12 h to 4 days, and each of the cases is associated with heavy precipitation and flooding. The Fella2003 case accumulated 343 mm maximum rainfall within 12 h with ~20% of the hourly rain rates exceeding 10 mm. The impact of this heavy precipitation was enhanced by the complex terrain resulting in a series of subsequent hazards (floods and landslides) over the Fella basin. The two Sesia cases reached maximum rainfall accumulations of 253 mm and 353 mm, respectively. The largest maximum rainfall accumulation out of the five events (409 mm) occurred in the Gard2008 case. This 2-day event had only small fraction (~5%) of the hourly rain rates greater than 10 mm h^{-1}, as the rain accumulation is due to a stationary mesoscale system that produced moderate rainfall rates. In comparison to the above cases, the Gard2007 event was relatively mild, occurring over a 4-day period and producing 294 mm of maximum rainfall accumulation. It is noted that most of the rain accumulation of Gard2007 occurred in the last 20 h of the event. Therefore, the rainfall intensities in this event were high and triggered a destructive flash flood in the Gard basin.

The precipitation datasets for each storm case consisted of three sources: satellite rainfall from CMORPH, rain gauge–adjusted radar rainfall, and simulated rainfall fields from WRF. Table 2 summarizes the resolutions of each data source. A description of the satellite and radar data is given below, and the WRF simulations are discussed in the next section.

CMORPH is a satellite rainfall algorithm that uses motion vectors derived from half-hourly interval geostationary satellite IR imagery to propagate the relatively high-quality rainfall estimates obtained from Earth-orbiting satellite–based passive microwave (PMW) sensors (Joyce et al. 2004). The dynamic morphological characteristics (such as shape and intensity) of the precipitation features are morphed at consecutive times between PMW sensor samples by performing a time-weighted linear interpolation. This process yields spatially and temporally continuous PMW rainfall fields that have been guided by IR imagery and yet is independent of any IR temperature–based inversion to rainfall rate (Kidd et al. 2012). However, there are certain issues with the technique as highlighted by Joyce et al. (2004): (i) the algorithm may miss precipitation that forms and develops over an area between PMW overpasses and (ii) the current snow-screening process gives nonzero rainfall estimates to the snow or ice areas, thus causing inauthentic observations over these areas that are usually associated with high elevations and mountainous terrain. These deficiencies introduce uncertainties to the CMORPH precipitation estimates, which propagate in flood prediction when these estimates are used as input to a hydrologic model. Nevertheless, as indicated by several satellite error studies (Stampoulis and Anagnostou 2012; Kidd et al. 2012; Bitew et al. 2012; Dinku et al. 2007), CMORPH retrieval

TABLE 3. WRF simulation domain setting.

			Fella2003	Sesia2005	Sesia2006	Gard2007	Gard2008
First domain	Number of grid points	*x*, *y*	156, 120	156, 120	156,120	156, 120	156, 120
	Lon (°E)	Min	−10.41	−12.45	−13.7	−16.45	−16.45
		Max	33.31	30.45	28.6	24.53	24.53
	Lat (°N)	Min	36.19	35.42	34.84	33.5	33.5
		Max	56.59	55.79	55.19	53.8	53.8
Second domain	Number of grid points	*x*, *y*	216, 123	216, 123	390, 270	252, 198	252, 198
	Lon (°E)	Min	2.6	0.3	−10.48	−6.08	−6.08
		Max	20.8	18.2	23.35	14.65	14.65
	Lat (°N)	Min	43.8	43.01	37.24	38.69	38.69
		Max	50.69	49.89	52.68	49.68	49.68
Third domain	Number of grid points	*x*, *y*	258, 171	258, 222	1020, 690	408, 336	408, 336
	Lon (°E)	Min	8.14	5.69	−7.64	−1.03	−1.03
		Max	15.08	12.64	21.21	9.75	9.75
	Lat (°N)	Min	45.18	44.38	38.21	41.24	41.24
		Max	48.29	48.4	51.3	47.38	47.38

TABLE 4. WRF parameterizations.

WRF parameter	Scheme
Microphysics	New Thompson et al. (2008) scheme: a new scheme with ice, snow, and graupel processes suitable for high-resolution simulations
Longwave radiation	Rapid Radiative Transfer Model scheme
Shortwave radiation	Dudhia scheme: simple downward integration efficiently allowing for clouds and clear-sky absorption and scattering
Surface layer	MM5 similarity: based on Monin–Obukhov with Carslon–Boland viscous sublayer and standard similarity functions from look-up tables*
Land surface	Five-layer thermal diffusion: soil temperature only scheme
Planetary boundary layer	Yonsei University scheme: nonlocal K scheme with explicit entrainment layer and parabolic K profile in unstable mixed layer
Cumulus parameterization	Kain–Fritsch cumulus parameterization on the parent and second domains; no parameterization on the third domain

* MM5 stands for fifth-generation Pennsylvania State University–National Center for Atmospheric Research Mesoscale Model.

exhibits a better consistency relative to other satellite products over complex terrain areas.

The radar rainfall data for the Fella storm case were obtained from a Doppler, dual-polarized C-band radar after converting the reflectivity scans to rainfall values via a rain gauge-calibrated Z–R relationship. Several procedures were applied to correct for ground clutter, partial beam blockage, and rain-path attenuation (Borga et al. 2007). The radar data for the Sesia cases were from the Bricdella Croce Doppler weather radar and the radar rainfall estimates were quality controlled and bias adjusted using rain gauge measurements (Sangati et al. 2009). The radar rainfall for the Gard storm cases were obtained using quantitative rainfall estimation procedures applied to weather radars of the Météo-France Association pour la Réalisation des Actions et des Missions Sociales (ARAMIS) network (Delrieu et al. 2005). The procedures include detailed radar data quality control and rain gauge–based bias adjustment of the radar rainfall estimates. Even though radar rainfall estimates are affected by error sources, for example, the effect of rainfall drop size distribution variability on the reflectivity-to-rainfall rate conversion, rain-path attenuation, and beam blockage effects, when postprocessing data quality control is performed, it can be considered a reliable data source for evaluating remote sensing rainfall product.

3. Numerical weather simulation model setup

The numerical weather simulations in this study were performed by the WRF modeling system, version 3.4 (Skamarock et al. 2008). By initializing the model with both the Global Forecast System (GFS) data and Local Analysis and Prediction System (LAPS) reanalysis data, WRF generated better simulations than using GFS analysis fields alone. GFS data are commonly used to initialize WRF simulation. The GFS data used in this study are in 1° spatial resolution and 6-h temporal resolution. The LAPS analysis data were provided every 3 h in the spatial resolution of 15 km. LAPS analysis represents a regional dataset covering a large portion of northern Africa, Europe, and major parts of the Atlantic Ocean. These data were generated in the framework of the European Union Climate Change and Impact Research: The Mediterranean Environment (CIRCE) project through the LAPS assimilation system (Albers et al. 1996) using the available observations from weather stations and buoys, along with the 0.5°/6-hourly European Centre for Medium-Range Weather Forecasts (ECMWF) analysis fields.

The WRF simulations have been performed in a two-way interactive mode with 35 vertical levels and a three-domain configuration, in which the coarsest spatial resolution is 18 km and two nested domains have the resolution of 6 km and 2 km, respectively. The domain

TABLE 5. Time period of WRF simulation.

WRF simulation	Fella2003	Sesia2005	Sesia2006	Gard2007	Gard2008
Starting time	29 Aug 2003 0000 UTC	1 Aug 2005 1200 UTC	13 Sep 2006 1800 UTC	19 Nov 2007 0000 UTC	31 Oct 2008 0000 UTC
Ending time	30 Aug 2003 1200 UTC	3 Aug 2005 0000 UTC	16 Sep 2006 0600 UTC	23 Nov 2007 1200 UTC	2 Nov 2008 1200 UTC
Duration (h)	36	36	60	108	60

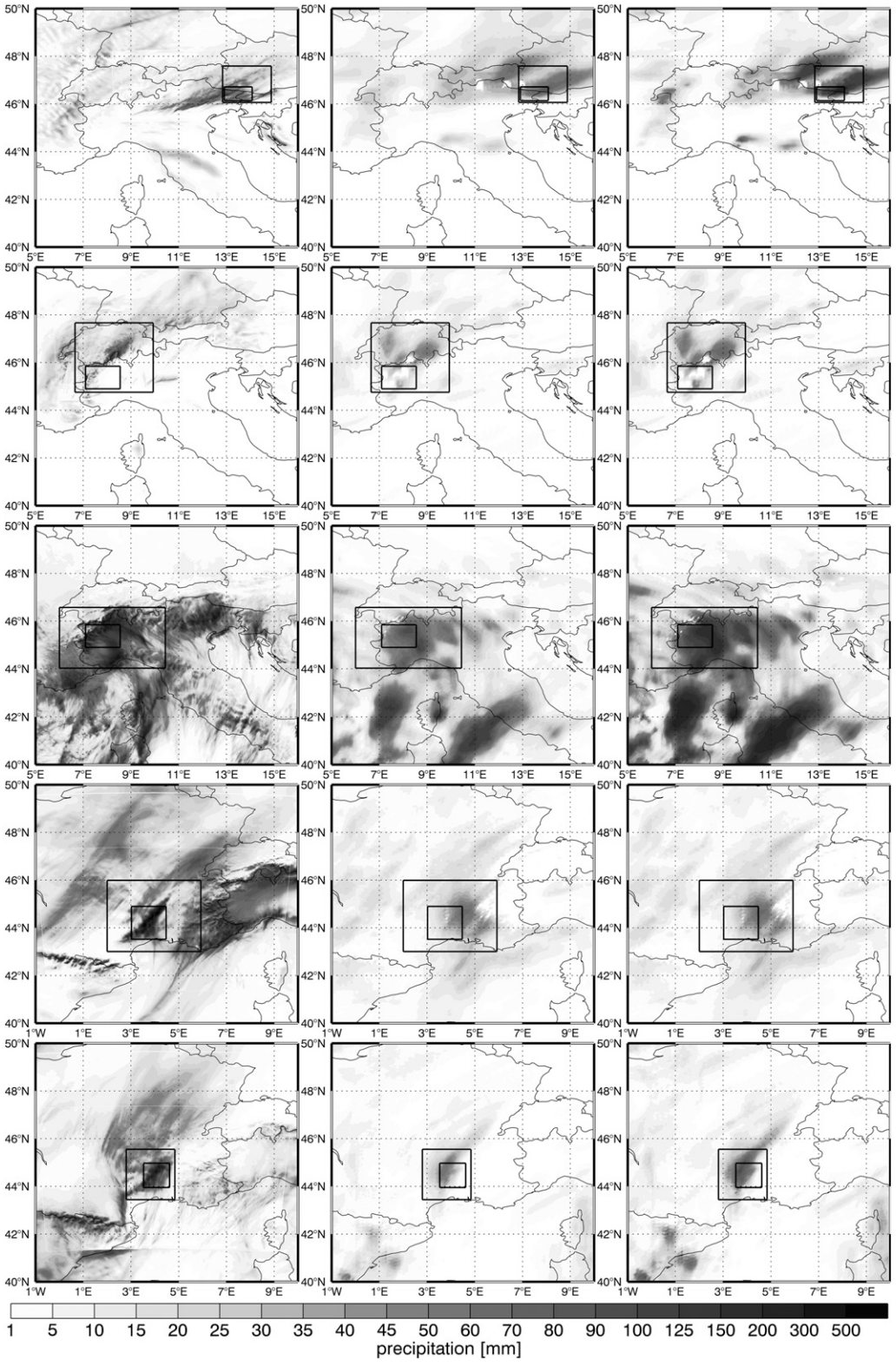

FIG. 2. Accumulated rainfall maps for each storm event. From top to bottom: Fella2003, Sesia2005, Sesia2006, Gard2007, and Gard2008. (left) WRF maps, (middle) CMOPRH maps, and (right) the adjusted CMORPH maps. The area encompassed by the outer rectangle box is the fitting domain; the area encompassed by the inner rectangle box is the radar domain for the error analyses.

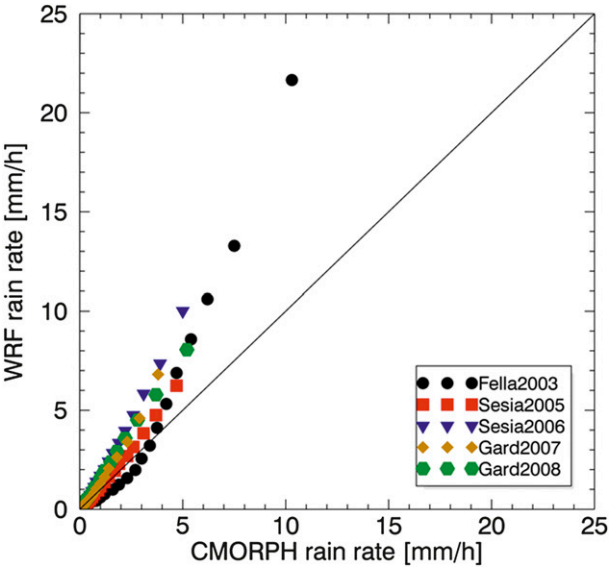

FIG. 3. Q–Q plot of WRF rate rates vs CMORPH rain rates.

sizes and locations are accommodated according to the different study regions. The geographic data used to define domains and interpolate terrestrial datasets are in 30-s resolution. Table 3 presents the domain setting for each storm case. The WRF parameterization scheme selection is based on findings from a WRF sensitivity study of Mediterranean rain events done by Laviola et al. (2011). Table 4 lists the parameterization schemes used in the model for microphysics, radiation, convection, boundary layer, and soil processes. These parameterizations are consistently implemented in the simulations of all five storm cases. Finally, Table 5 shows the WRF integration time periods for each storm case. The model output files were analyzed at hourly time intervals.

4. Methodology

In this section we describe the three main steps that constitute the procedure used for determining the adjustment for CMORPH estimates and evaluating those estimates against the in situ radar rainfall data.

a. Data processing

The first step was to bring all datasets into a common spatial and temporal resolution grid in order to determine the bias error statistic. The selected spatiotemporal scale was 8 km and 1 h, representing the coarsest resolution among the various datasets. For each storm case, two domains were defined for two distinct purposes: one is the fitting domain, where we determine the CMORPH rainfall adjustment parameters through comparison with WRF rainfall fields, and the second is the radar domain, which is used to determine the error statistics. The radar domains for the three study areas (Fella, Sesia, and Gard) are shown in Fig. 1.

TABLE 6. Fitting parameter values.

Parameter	Fella2003	Sesia2005	Sesia2006	Gard2007	Gard2008
a	0.37	1.12	1.68	1.32	1.56
b	1.79	1.09	1.09	1.19	1.02

b. CMORPH adjustment procedure

The CMORPH adjustment is based on a power-law function [shown in Eq. (1)], which is selected based on the WRF–CMORPH data relationships derived from the five storm cases:

$$Y = a \times X^b, \tag{1}$$

where X and Y represent the CMORPH and WRF hourly rain rates (in mm h^{-1}), respectively, and a and b are parameters to be estimated over the fitting domain. These two parameters have distinct values for each storm case. The procedure for estimating the parameters is as follows.

First, we define a fitting domain for each case. There are two criteria for selecting a fitting domain: (i) the domain should be small enough to focus on the area of the storm (see Fig. 1) and should therefore represent the distinctive precipitation features associated with the satellite retrieval, and (ii) the domain should be large enough to contain most of the intense rainfall areas and should take into account the numerical simulation misplacements. A fixed cumulative distribution function (CDF) bin with cumulative probability values ranging from 5% to 95% is defined to determine the corresponding WRF and CMORPH hourly rain rate quantiles. By using the least squares method, the adjustment function is then employed to fit these WRF versus CMOPRH hourly rain rate quantiles using Eq. (1) and thus determines the values for parameters a and b. Adjusted CMORPH hourly rain rates were then obtained by applying the adjustment function of Eq. (1) with the determined parameters on the original CMORPH rain rates. It is noted that the herein adjustment method does not correct for rainfall detection error, which may be a significant factor in satellite rainfall underestimation over mountainous areas.

c. Error analysis

The error analysis in this study is provided over the radar domain to independently evaluate the improvements obtained by the proposed adjustment. We devise

a number of error metrics determined between each estimator and the reference radar rainfall rates. The estimators are the original CMORPH products, adjusted CMORPH estimates, and WRF simulated rainfall. Besides the hourly rainfall time series and the Q–Q plot, two verification scores, which are the bias score (BS) and Heidke skill score (HSS), are implemented to present the performance of the estimators. To calculate these metrics, a set of hourly precipitation thresholds were created: 1, 2, 4, 8, and 12 mm. Then, by considering the following occurrences A, B, C, and D,

A: estimator > threshold and radar > threshold;
B: estimator > threshold and radar < threshold;
C: estimator < threshold and radar > threshold;
D: estimator < threshold and radar < threshold.

BS is defined as the ratio of the number of occurrences that estimated rain rates exceed a specified threshold versus the respective number from the reference rain rates:

$$\mathrm{BS} = \frac{A + B}{A + C}. \tag{2}$$

HSS (Heidke 1926) is defined as the number of correct estimated occurrences minus the number of correct estimated occurrences by chance divided by the total number of estimated occurrences minus the number of correct estimated occurrences by chance:

$$\mathrm{HSS} = \frac{(A + D) - \dfrac{(A + B)(A + C) + (B + D)(C + D)}{(A + B + C + D)}}{(A + B + C + D) - \dfrac{(A + B)(A + C) + (B + D)(C + D)}{(A + B + C + D)}}. \tag{3}$$

Eq. (3) can be simplified to

$$\mathrm{HSS} = \frac{2(A \times D - B \times C)}{(A + C)(C + D) + (A + B)(B + D)}. \tag{4}$$

Technically, the range of HSS is $-\infty$ to 1. A perfect precipitation estimator would obtain an HSS value equal to 1, while HSS less than or equal to zero indicates that the technique gives mostly a random estimation or has fewer hits than a random estimation. HSS is a widely used score because it is fairly easy to compute and it may explain more than one effect such as probability of detection, false alarm rate, and occurrences by chance.

5. Results

The five storm cases analyzed in this study are distinct in terms of the rainfall intensities and the spatiotemporal rain structures, which provide a good representation of the heavy storm types occurring in complex terrain areas. Overall, the 2-km resolution WRF and 8-km resolution CMORPH rainfall accumulations (Figs. 2a,b) show similar patterns for the different storm cases. The Q–Q plot of WRF versus CMORPH rain rates (Fig. 3) consistently exhibits approximate power-law relationships; thus the power-law-fitting equation [Eq. (1)] is selected to adjust CMORPH rainfall estimates. Specifically, the Sesia and Gard cases group together with less nonlinear shapes, while the Fella2003 case displays a strong power-law curve. As a consequence, the parameter values of Eq. (1) are within a narrow range for all storm events except Fella2003 (Table 6). In Sesia and Gard cases, parameter a is between 1.12 and 1.68 and parameter b is between 1.02 and 1.19. In the Fella2003 case, the a value is much smaller and b value is much larger than the other cases.

The adjustment of CMORPH estimates demonstrates improvement in terms of rainfall magnitude (Fig. 2). For the purpose of verifying CMORPH's actual improvement, the independent radar-derived rainfall estimation was introduced as a reference dataset to compare with the three estimators. The results for each storm case are described next.

a. *Fella2003 case*

The Fella2003 case lasted only 12 h, with very intense rainfall mostly concentrated in the afternoon of 29 August 2003. Considering a threshold of 0.1 mm h^{-1} as the minimum value of CMORPH effective rain rate, it is found that a very low percentage (1.2%) of the radar precipitation was not detected by CMORPH. The high rain detection for this storm indicates that the CMORPH observation indeed captured the main features of the Fella2003 rainfall system, which explains why the adjustment procedure gave the best results in terms of overall bias correction. Figure 4a shows the Q–Q plot of radar rainfall versus the different rainfall estimators, which substantiates the claim that the adjusted CMORPH rainfall has the best consistency with the reference radar data among the three estimators.

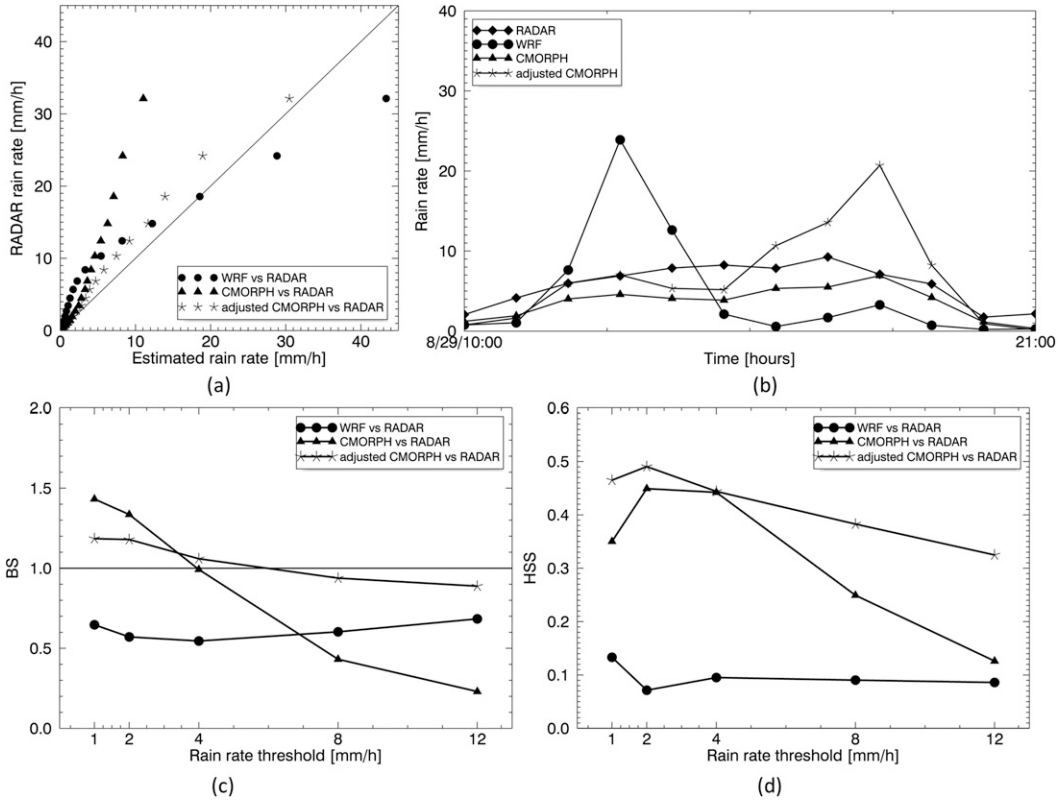

FIG. 4. Validation results over the radar domain for the Fella2003 case. (a) Q–Q plot of estimated rain rates vs radar rain rates, (b) hourly rainfall time series, (c) BS for different rain rate thresholds, and (d) HSS for different rain rate thresholds.

In addition, the BSs in Fig. 4c and HSSs in Fig. 4d are introduced to test the details of the CMORPH adjustment at different hourly rainfall thresholds. Both the BS and HSS can test the occurrences of estimators exceeding or failing to reach a certain precipitation threshold, while the HSS also provides combined assessment of the probability of detection and false alarm rate. The BS values of adjusted CMORPH are closest to 1 compared to the other two estimators, meaning that adjusted CMORPH estimation has more similar occurrences with the radar data, especially when the rainfall threshold is greater than 4 mm h^{-1}. Moreover, the HSS plot shows the highest values (around 0.4) in the adjusted CMORPH data and lowest values in WRF simulations, which indicates that the adjusted CMORPH hourly rainfall data perform best not only on rainfall occurrences, but also in terms of rainfall magnitudes, while WRF data give the least accuracy for the rainfall detection at almost all precipitation thresholds.

The conclusion about rainfall detection is confirmed in Fig. 4b, depicting the hourly rainfall time series plot. It is apparent that the radar rainfall peak is not captured correctly by the WRF simulations. WRF generates the peak time ~3 h earlier and shows very low value at the actual peak. The CMOPRH peak is only 1 h later than the radar peak and follows a similar trend as the radar data. Furthermore, it is important to note that the CMORPH adjustment does not provide enough increase for the low rainfall values, while the improvement is significant for the high rainfall values such as the rainfall rate at the peak time. Overall, for the Fella2003 event, the adjusted CMORPH estimation is better than both the original CMORPH and WRF simulations in terms of the representation of area rainfall dynamics. Therefore, for this storm case, the high-resolution storm simulation from WRF improved the CMORPH rain estimation performance by reducing the strong underestimation of high rainfall rates.

b. *Sesia2005 case*

The Sesia2005 event started in the evening of 1 August 2005 and lasted 24 h, producing moderate rainfall rates. There was only 32% of radar rainfall detected by the

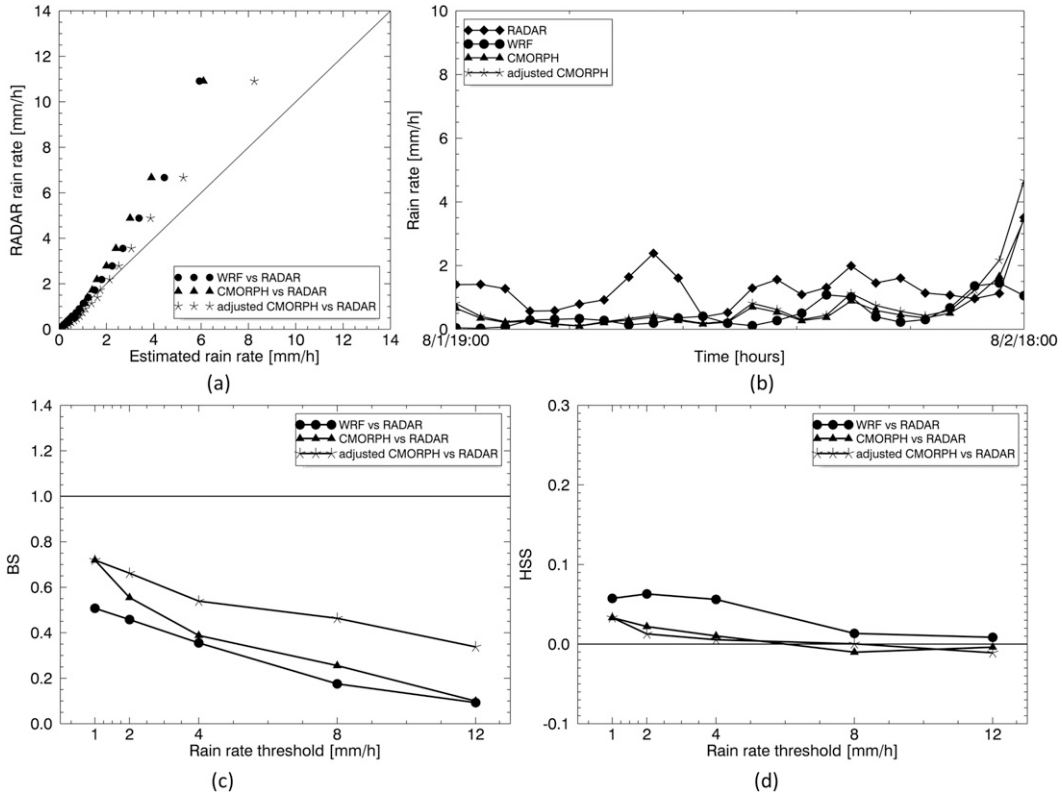

FIG. 5. As in Fig. 4, but for the Sesia2005 case.

CMORPH estimates, which makes the adjustment less efficient than in the case of Fella2003. Although the Q–Q plot over the radar domain (Fig. 5a) illustrates that the adjusted CMORPH performs best among the three estimators, the CMORPH improvement is still not enough and exhibits large underestimation. The improvement was further evidenced by the bias scores (Fig. 5c), in which the adjusted CMORPH exhibited better consistency with radar rainfall than either WRF or the original CMORPH estimates, especially for rainfall rates above the high rain rate thresholds. However, the HSS (Fig. 5d) of CMORPH and adjusted CMORPH data is around zero, which means that both CMORPH estimators are associated with high random error. This points out that the CMORPH detection problem dominated the estimation inaccuracy for this storm.

Furthermore, a plot of hourly rainfall time series (Fig. 5b) shows that WRF-simulated rainfall tends to develop the rain peak earlier than the actual peak time. On the other hand, CMORPH and adjusted CMORPH rainfall follow the reference time series better since they observed several rainfall peaks at the same time as the radar data. However, the original CMORPH data are too low to provide a reasonable estimation and the adjusted CMORPH data did not obtain enough improvements from the WRF-based adjustment.

c. *Sesia2006 case*

The Sesia2006 storm event started at 0000 UTC on 14 September 2006 and persisted for 2 days. The WRF simulation for this event provided a good estimation of rainfall magnitude compared to radar (Fig. 6a), while the CMORPH data exhibited significant underestimation. The adjusted CMORPH rain rates obtained substantial improvement results for the high rain rates, while lower rain rates (less than $8\,\mathrm{mm\,h^{-1}}$) did not increase enough to reach the reference values. Figure 6c shows that the BS of the adjusted CMORPH data is consistently close to 1, which indicates that the adjustment reduced the dependency of CMORPH bias on rain magnitude. In addition, the BS of adjusted CMORPH data provides particularly good estimation for the larger rain rate thresholds, but it performs less accurately than WRF for the lower thresholds. Moreover, as shown in Fig. 2, CMORPH rainfall patterns are different than the radar rainfall for this event, which can be due to effects of snow land cover on the PMW retrieval. Because of these spatial pattern mismatches, the HSS plot of the

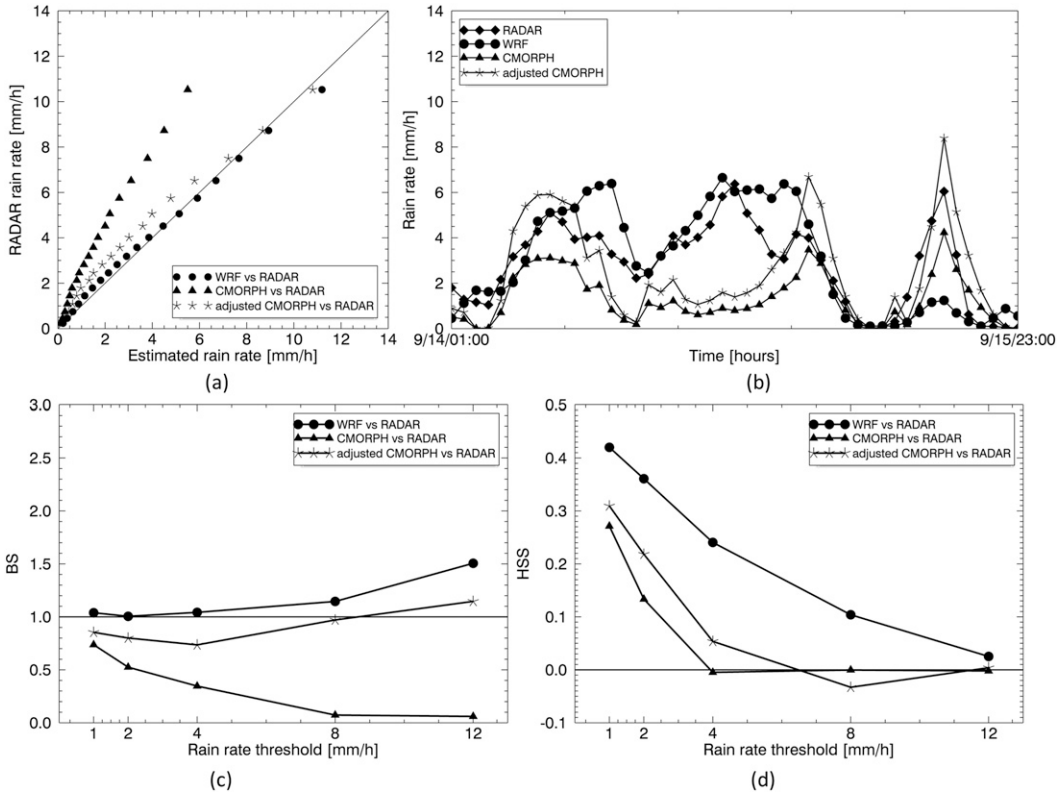

FIG. 6. As in Fig. 4, but for the Sesia2006 case.

CMORPH estimates (Fig. 6d) does not show apparent improvements from the WRF-based adjustment. The hourly rainfall time series (Fig. 6b), on the other hand, demonstrate that the adjusted CMORPH rainfall exhibits improvement over the original CMORPH estimates, with rainfall magnitudes and dynamics following closer the reference radar rainfall data.

d. Gard2007 case

Gard2007 was the longest-lived precipitation event among the five storm cases used in this study. This event lasted almost 4 days. The extreme portion of the storm, however, did not occur until the last 20 h. The storm event is located at the windward slope of the Massif Central mountain range. WRF has considered this topographic factor and consistently simulated the rainfall distribution map (Fig. 2) with a very clear boundary between the precipitation concentrated area and the mountain leeward. The CMORPH rainfall estimates for this event exhibit a slight spatial shift to the east and do not show a clear rainband as in the WRF analysis.

Figure 7a shows improvement due to the adjusted CMORPH rainfall estimates relative to radar data. However, since this Q–Q plot is based on conditional rain rates, it does not represent the overall performance of the estimator. Hence, it is understandable that the adjusted CMORPH data exhibit only slight improvement in the BS plot (Fig. 7c). The HSS plot (Fig. 7d) shows the lowest (highest) scores for the WRF (adjusted CMORPH) data. This is also apparent in the time series plots (Fig. 7b). Although WRF has similar amounts in terms of accumulated rainfall to the radar data, these values come at different peak times, which cause the low HSS values. On the other hand, the adjusted CMORPH data detected the major rainfall peaks well.

e. Gard2008 case

Gard2008 case was a 2-day rainfall event. It ended after the maximum rainfall peak time. Although the Q–Q plot over the radar domain (Fig. 8a) shows significant improvement of the adjusted CMORPH data relative to the original CMORPH estimates, the hourly rainfall time series (Fig. 8b) indicates that the missed detection of CMORPH rain rates cannot be meliorated by the adjustment procedure. Again, this is due to the fact that there is nearly 70% of CMORPH hourly rainfall

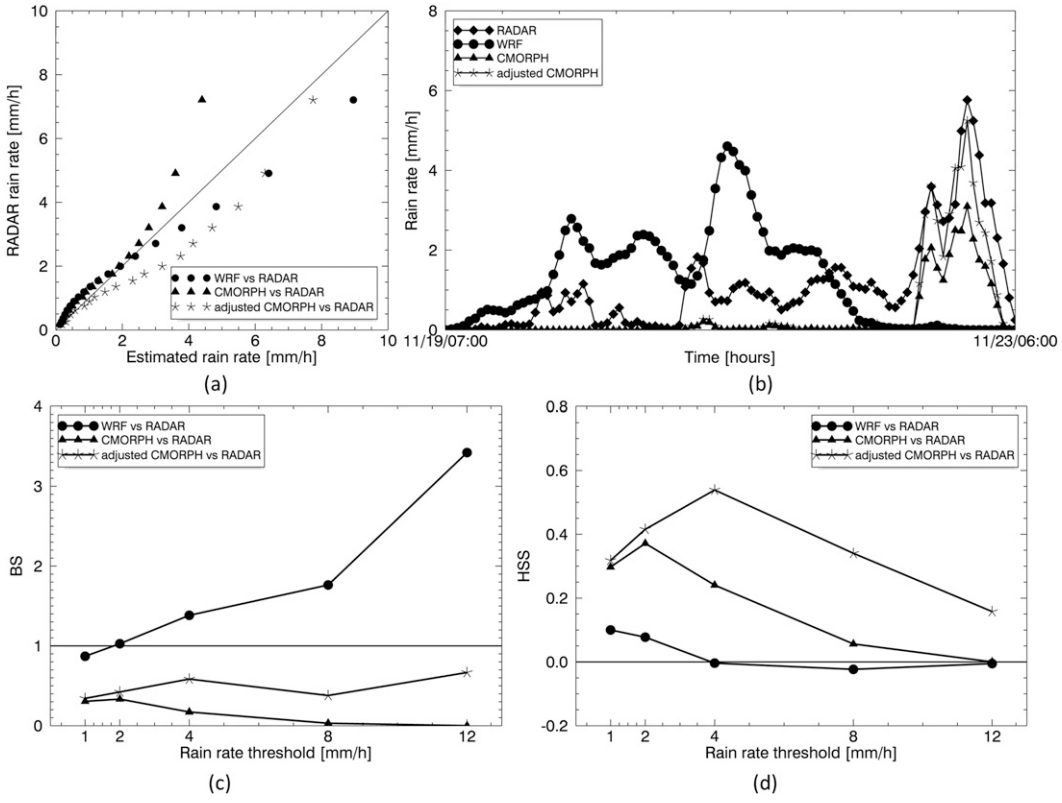

FIG. 7. As in Fig. 4, but for the Gard2007 case.

estimates over the radar domain with values less than 0.1 mm h^{-1}. The adjustment brought slight improvement in those low rainfall rates. The BS plot (Fig. 8c) also illustrates that the improvement of adjusted CMORPH data is insufficient to reduce the overall underestimation. The adjusted CMORPH data outperformed the other two estimators in the HSS metric (Fig. 8d), especially for the rainfall rates above the higher rain rate thresholds.

6. Conclusions

This study investigated the use of high-resolution (2 km) simulations performed with WRF in determining heavy precipitation biases of satellite rain retrievals (i.e., CMORPH in this study) over complex terrain areas. The study focused on five heavy precipitation events over southern Europe (northern Italy and southern France). Quality-controlled radar rainfall data were used as reference rainfall to evaluate improvements obtained on CMORPH rainfall estimates using WRF-based adjustments.

It was shown that CMORPH has a tendency to substantially underestimate the rainfall magnitudes of the examined heavy precipitation events. The analysis also confirmed the fact that rainfall estimates from CMORPH do not detect very low rain rates. On the other hand, CMORPH was shown to perform well in capturing the storm dynamics including the occurrence of the major rain rate peaks. The high-resolution (2 km) rainfall simulations from WRF provided relatively accurate quantification of the storm rain accumulations and of the conditional (nonzero) rain rate distributions for the examined storm cases. However, significant time differences were exhibited between WRF and radar rainfall peaks. Using the high-resolution WRF simulations for adjusting CMORPH estimates, we could demonstrate improvements in the CMORPH rainfall error statistics relative to the original CMORPH estimates or the WRF rainfall simulations alone. Adjustments to the CMORPH rainfall estimates were applied using a power-law relationship with parameters determined on a storm-to-storm basis. The main points on the CMORPH adjustment performance based on the five storm cases examined in this study are summarized below.

The adjusted CMORPH hourly rain rates exhibited significant improvements when the original CMORPH estimates represented rainfall with high detection accuracy. The missed rainfall rates in the original CMORPH estimates limited the impact of the proposed adjustment technique on improving the overall bias in the CMORPH

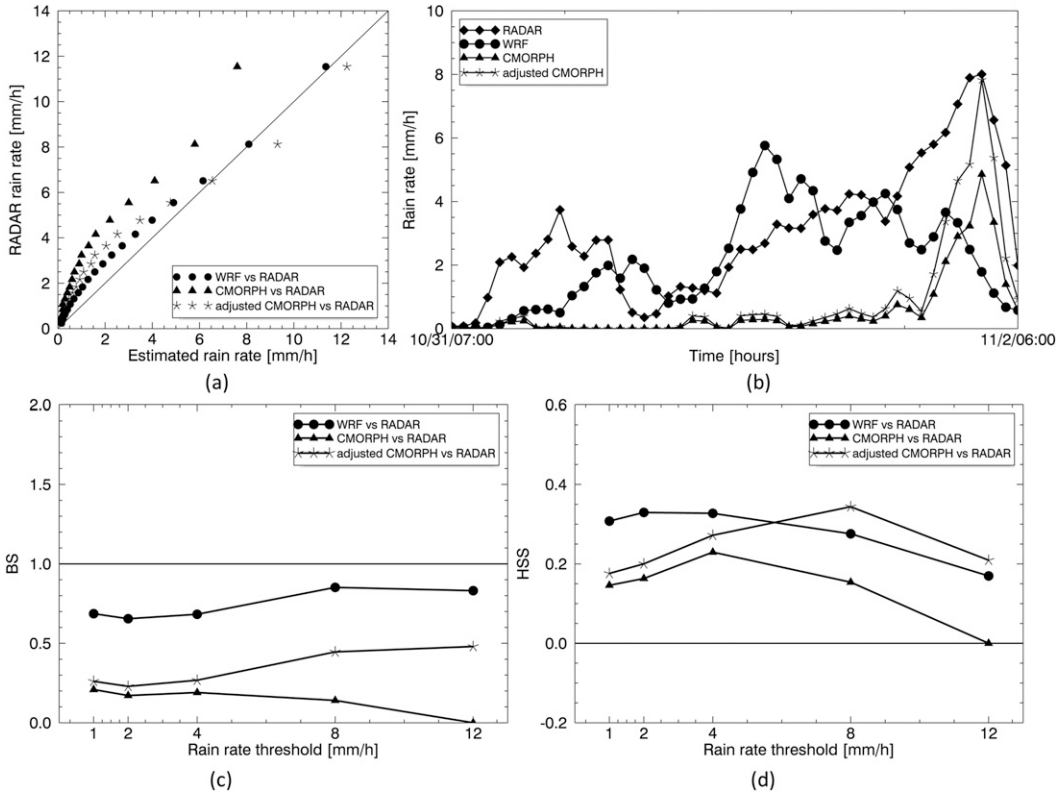

FIG. 8. As in Fig. 4, but for the Gard2008 case.

rainfall product. Among the five storm events examined here, the CMORPH estimates of Fella2003 case had the least missed rainfall. This storm case exhibited the greatest improvement in the CMORPH rainfall estimation because of the WRF-based adjustment.

The adjustment was shown to provide the most significant improvement for the higher rainfall rates, for which CMORPH usually exhibits significant underestimation. Only slight improvement was shown for the low rain rates. In all storm cases, the bias scores of the original CMORPH estimates exhibited strong rain rate magnitude dependence. After adjustment, this magnitude dependence was moderated, leading to a more consistent estimate.

Overall, the adjusted CMORPH rainfall performed consistently better than the original CMORPH data. Furthermore, in Fella2003, Gard2007, and Gard2008 the adjusted CMORPH rainfall provided better estimation than the WRF simulations in terms of the HSS skill scores examined in this study, which indicates that the WRF-adjusted satellite rainfall product can be superior to the high-resolution WRF simulations when it comes to capturing the hydrologic variability.

This research only accounted for the conditional error focusing on a limited number (five) of heavy precipitation events. Future extensions should investigate dependencies on model microphysics, resolution, and include other satellite retrieval techniques as well as additional heavy precipitation cases. One of the limiting factors of this adjustment procedure is the detection of rainfall by the various satellite rainfall techniques. Therefore, an important aspect to be investigated in future studies is how to use the weather model simulations to improve the characterization of satellite rainfall detection error. Furthermore, given that future high-frequency passive microwave satellite rainfall techniques associated with the Global Precipitation Measurement (GPM) mission are going to improve the rainfall detection problem, one would expect a better efficiency of the proposed model-based adjustment procedure. This aspect needs to be confirmed using new satellite rainfall products as algorithms are transitioning to the GPM observation era.

Acknowledgments. This work was supported by a NASA Precipitation Measurement Mission award (NNX07AE31G). We also acknowledge and appreciate Prof. Marco Borga of the University of Padova and Prof. Guy Delrieu of the Laboratoire d'Etude des Transferts en Hydrologie et Environnement (LTHE)

for providing the radar rainfall data for the flood cases in the Italian and French basins, respectively.

REFERENCES

Albers, S. C., J. A. McGinley, D. L. Birkenheuer, and J. R. Smart, 1996: The Local Analysis and Prediction System (LAPS): Analyses of clouds, precipitation, and temperature. *Wea. Forecasting,* **11,** 273–287, doi:10.1175/1520-0434(1996)011<0273:TLAAPS>2.0.CO;2.

Bitew, M. M., M. Gebremichael, L. T. Ghebremichael, and Y. A. Bayissa, 2012: Evaluation of high-resolution satellite rainfall products through streamflow simulation in a hydrological modeling of a small mountainous watershed in Ethiopia. *J. Hydrometeor.,* **13,** 338–350, doi:10.1175/2011JHM1292.1.

Borga, M., P. Boscolo, F. Zanon, and M. Sangati, 2007: Hydrometeorological analysis of the 29 August 2003 flash flood in the eastern Italian Alps. *J. Hydrometeor.,* **8,** 1049–1067, doi:10.1175/JHM593.1.

Bray, M., D. Han, Y. Xuan, P. Bates, and M. Williams, 2011: Rainfall uncertainty for extreme events in NWP downscaling model. *Hydrol. Processes,* **25,** 1397–1406, doi:10.1002/hyp.7905.

Delrieu, G., and Coauthors, 2005: The catastrophic flash-flood event of 8–9 September 2002 in the Gard region, France: A first case study for the Cévennes–Vivarais Mediterranean Hydrometeorological Observatory. *J. Hydrometeor.,* **6,** 34–52, doi:10.1175/JHM-400.1.

Dinku, T., P. Ceccato, E. Grover-Kopec, M. Lemma, S. J. Connor, and C. F. Ropelewski, 2007: Validation of satellite rainfall products over East Africa's complex topography. *Int. J. Remote Sens.,* **28,** 1503–1526, doi:10.1080/01431160600954688.

Ebert, E. E., J. E. Janowiak, and C. Kidd, 2007: Comparison of near-real-time precipitation estimations from satellite observations and numerical models. *Bull. Amer. Meteor. Soc.,* **88,** 47–64, doi:10.1175/BAMS-88-1-47.

Frei, C., and C. Schar, 1998: A precipitation climatology of the Alps from high-resolution rain-gauge observations. *Int. J. Climatol.,* **18,** 873–900, doi:10.1002/(SICI)1097-0088(19980630)18:8<873::AID-JOC255>3.0.CO;2-9.

Heidke, P., 1926: Berechnung des erfolges und der gute der windstarkevorhersagen im sturmwarnungsdienst. *Georg. Ann.,* **8,** 310–349.

Huffman, G. J., R. F. Adler, B. Rudolf, U. Schneider, and P. R. Keehn, 1995: Global precipitation estimates based on a technique for combining satellite-based estimates, rain gauge analysis, and N WP model precipitation information. *J. Climate,* **8,** 1284–1295, doi:10.1175/1520-0442(1995)008<1284:GPEBOA>2.0.CO;2.

Joyce, R. J., J. E. Janowiak, P. A. Arkin, and P. Xie, 2004: CMORPH: A method that produces global precipitation estimates from passive microwave and infrared data at high spatial and temporal resolution. *J. Hydrometeor.,* **5,** 487–503, doi:10.1175/1525-7541(2004)005<0487:CAMTPG>2.0.CO;2.

Kidd, C., P. Bauer, J. Turk, G. J. Huffman, R. Joyce, K.-L. Hsu, and D. Braithwaite, 2012: Intercomparison of high-resolution precipitation products over northwest Europe. *J. Hydrometeor.,* **13,** 67–83, doi:10.1175/JHM-D-11-042.1.

Laviola, S., A. Moscatello, M. M. Miglietta, E. Cattani, and V. Levizzani, 2011: Satellite and numerical model investigation of two heavy rain events over the central Mediterranean. *J. Hydrometeor.,* **12,** 634–649, doi:10.1175/2011JHM1257.1.

Lionello, P., and Coauthors, 2006: The Mediterranean climate: an overview of the main characteristics and issues. *Mediterranean,* P. Lionello, P. Malanotte-Rizzoli, and R. Boscolo, Eds., Developments in Earth and Environmental Sciences, Vol. 4, Elsevier, 1–26, doi:10.1016/S1571-9197(06)80003-0.

Maddox, R. A., J. Zhang, J. J. Gourley, and K. W. Howard, 2002: Weather radar coverage over the contiguous United States. *Wea. Forecasting,* **17,** 927–934, doi:10.1175/1520-0434(2002)017<0927:WRCOTC>2.0.CO;2.

Malguzzi, P., G. Grossi, A. Buzzi, R. Ranzi, and R. Buizza, 2006: The 1966 ''century'' flood in Italy: A meteorological and hydrological revisitation. *J. Geophys. Res.,* **111,** D24106, doi:10.1029/2006JD007111.

Mehta, A. V., and S. Yang, 2008: Precipitation climatology over Mediterranean basin from ten years of TRMM measurements. *Adv. Geosci.,* **17,** 87–91, doi:10.5194/adgeo-17-87-2008.

Nikolopoulos, E. I., and E. N. Anagnostou, 2010: Understanding the scale relationships of uncertainty propagation of satellite rainfall through a distributed hydrologic model. *J. Hydrometeor.,* **11,** 520–532, doi:10.1175/2009JHM1169.1.

——, ——, and M. Borga, 2012: Using high-resolution satellite rainfall products to simulate a major flash flood event in northern Italy. *J. Hydrometeor.,* **14,** 171–185, doi:10.1175/JHM-D-12-09.1.

Nuissier, O., V. Ducrocq, D. Ricard, C. Lebeaupin, and S. Anquetin, 2008: A numerical study of three catastrophic precipitating events over southern France. I: Numerical framework and synoptic ingredients. *Quart. J. Roy. Meteor. Soc.,* **134,** 111–130, doi:10.1002/qj.200.

Papadopoulos, A., E. Serpetzoglou, and E. Anagnostou, 2008: Improving NWP through radar-rainfall-driven land surface parameters: A case study on convective precipitation forecasting. *Adv. Water Resour.,* **31,** 1456–1469, doi:10.1016/j.advwatres.2008.02.001.

Petrucci, O., and M. Polemio, 2009: The role of meteorological and climatic conditions in the occurrence of damaging hydrogeologic events in southern Italy. *Nat. Hazards Earth Syst. Sci.,* **9,** 105–118, doi:10.5194/nhess-9-105-2009.

Prat, O. P., and A. P. Barros, 2010: Assessing satellite-based precipitation estimates in the southern Appalachian Mountains using rain gauges and TRMM PR. *Adv. Geosci.,* **25,** 143–153, doi:10.5194/adgeo-25-143-2010.

Ruin, I., J.-D. Creutin, S. Anquetin, and C. Lutoff, 2008: Human exposure to flash floods—Relation between flood parameters and human vulnerability during a storm of September 2002 in southern France. *J. Hydrol.,* **361,** 199–213, doi:10.1016/j.jhydrol.2008.07.044.

Sangati, M., M. Borga, D. Rabuffetti, and R. Bechini, 2009: Influence of rainfall and soil properties spatial aggregation on extreme flash flood response modelling: An evaluation based on the Sesia River basin, north western Italy. *Adv. Water Resour.,* **32,** 1090–1106, doi:10.1016/j.advwatres.2008.12.007.

Schelfaut, K., B. Pannemans, I. van der Craats, J. Krywkow, J. Mysiak, and J. Cools, 2011: Bringing flood resilience into practice: The FREEMAN project. *Environ. Sci. Policy,* **14,** 825–833, doi:10.1016/j.envsci.2011.02.009.

Schwartz, C. S., and Coauthors, 2010: Toward improved convection-allowing ensembles: Model physics sensitivities and optimizing probabilistic guidance with small ensemble membership. *Wea. Forecasting,* **25,** 263–280, doi:10.1175/2009WAF2222267.1.

Skamarock, W. C., and Coauthors, 2008: A description of the Advanced Research WRF version 3. NCAR Tech. Note

NCAR/TN-475+STR, 113 pp. [Available online at http://www.mmm.ucar.edu/wrf/users/docs/arw_v3.pdf.]

Stampoulis, D., and E. N. Anagnostou, 2012: Evaluation of global satellite rainfall products over continental Europe. *J. Hydrometeor,* **13,** 588–603.

Tang, L., and F. Hossain, 2012: Investigating the similarity of satellite rainfall error metrics as a function of Köppen climate classification. *Atmos. Res.,* **104–105,** 182–192, doi:10.1016/j.atmosres.2011.10.006.

Thompson, G., P. R. Field, R. M. Rasmussen, and W. D. Hall, 2008: Explicit forecasts of winter precipitation using an improved bulk microphysics scheme. Part II: Implementation of a new snow parameterization. *Mon. Wea. Rev.,* **136,** 5095–5115.

Zupanski, D., S. Q. Zhang, M. Zupanski, A. Y. Hou, and S. H. Cheung, 2011: A prototype WRF-based ensemble data assimilation system for dynamically downscaling satellite precipitation observations. *J. Hydrometeor.,* **12,** 118–134, doi:10.1175/2010JHM1271.1.